

# IAIFNET: AN ILLUMINATION-AWARE INFRARED AND VISIBLE IMAGE FUSION NETWORK

Qiao Yang<sup>1</sup>, Yu Zhang<sup>2</sup>, Jian Zhang<sup>1,\*</sup>, Zijing Zhao<sup>1</sup>,  
Shunli Zhang<sup>1</sup>, Jinqiao Wang<sup>1</sup>, Junzhe Chen<sup>1</sup>

1. School of Software Engineering, Beijing Jiaotong University, China
2. School of Astronautics, Beihang University, China

## ABSTRACT

Infrared and visible image fusion (IVIF) is used to generate fusion images with comprehensive features of both images, which is beneficial for downstream vision tasks. However, current methods rarely consider the illumination condition in low-light environments, and the targets in the fused images are often not prominent. To address the above issues, we propose an Illumination-Aware Infrared and Visible Image Fusion Network, named as IAIFNet. In our framework, an illumination enhancement network first estimates the incident illumination maps of input images. Afterwards, with the help of proposed adaptive differential fusion module (ADFM) and salient target aware module (STAM), an image fusion network effectively integrates the salient features of the illumination-enhanced infrared and visible images into a fusion image of high visual quality. Extensive experimental results verify that our method outperforms five state-of-the-art methods of fusing infrared and visible images.

**Index Terms**— Image fusion, illumination enhancement, adaptive differential fusion

## 1. INTRODUCTION

In the field of image fusion, IVIF has been widely studied. Specifically, infrared images capture and reflect the thermal radiation emitted from objects, making them suitable for detecting hidden targets. However, infrared images often lack significant textural details of the scene. In contrast, visible images contain the majority of visual information within a supervised scene, making them highly suitable for perception by the human visual system [1]. Hence, the integration of the complementary features from the infrared and visible image into a single fusion image is of utmost importance in fully comprehending the supervised scene. Although IVIF has been widely studied and applied in domains such as military, semantic segmentation and target detection, it continues to pose a significant challenge due to the low-quality images captured in low-light environments.

Recently, a few methods were proposed to restore details in dark regions of fused images. To obtain fused images with

adaptive brightness, PIA [2] balanced the brightness information from different source images by considering the illumination contribution. DIVFusion [3] addressed the visual degradation defect of fused images in low-light environments by the Retinex theory, according to which the observed image  $I$  can be decomposed as

$$I = L \cdot R, \quad (1)$$

where  $L$  and  $R$  represent the incident illumination map and the reflection map, respectively. Although these works have achieved promising performance, there are still some drawbacks: i) In the low-light environment, existing methods cannot efficiently balance the illumination characteristics of infrared and visible images to obtain high-quality fused images. ii) The difference between multiple modalities may be large in extreme environments, introducing lots of noise or color distortion in the fused images.

To address the above challenges, we propose a novel infrared and visible image fusion framework based on illumination enhancement, namely IAIFNet. The main contributions are mainly threefold:

- We propose a novel infrared and visible image fusion framework, which exploits illumination-aware information to effectively generate a fusion image of appropriate brightness and contrast.
- We design two novel modules, i.e., an adaptive differential fusion module (ADFM) and a salient target aware module (STAM), in particular to solve the issues caused by the incident light, alleviating the influence of under-exposure or over-exposure and enhancing the salient targets in the fused image.
- The proposed network is designed in a lightweight manner, thus it can fast fuse infrared and visible images.

## 2. PROPOSED METHOD

### 2.1. Overall Architecture

Fig. 1 illustrates the overall architecture of our image fusion framework with ADFM and STAM. In the illumination en-

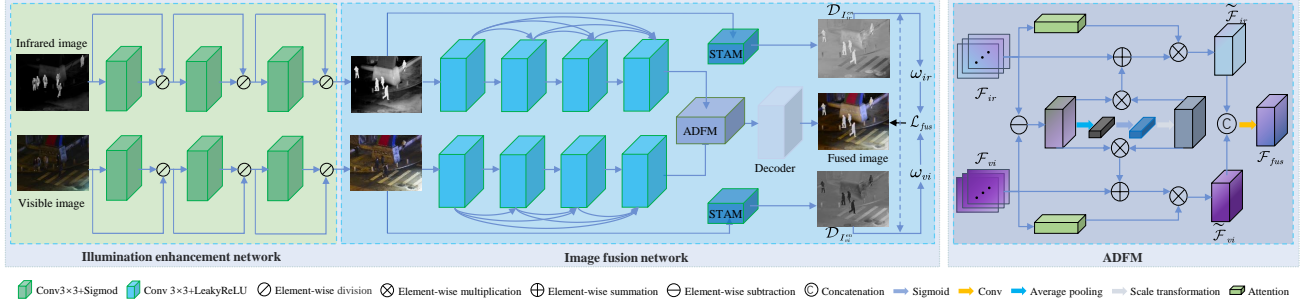


**Fig. 1.** Overall architecture of our method. The IAIFNet consists of two parts, the Illumination enhancement network and the Image fusion network. Detailed structure of the major component - ADFM, is also illustrated on the right.

ancement network, the sequential convolutional layers with sigmoid activation function extract the illumination-aware features from infrared and visible images through a residual connection based on Retinex theory. According to the generated distinct illumination-related features, the enhanced images can be further obtained. In the image fusion network, the sequential convolutional layers with leakyReLU activation function use the skip connection to extract multiple levels of feature maps, while ADFM is designed to integrate complementary and differential information in these feature maps. Then STAM captures the salient target area from the enhanced images. Finally, the integrated feature is fed into the subsequent decoder to reconstruct the fusion image. It is notable that IAIFNet is a lightweight network with a small number of parameters, enabling fast inference speed.

## 2.2. Detailed Networks

**Illumination Enhancement Network.** As the infrared and visible images are simultaneously taken at the same location, their illumination conditions can be regarded as the same. Inspired by [4], we leverage a single network to estimate the illumination map for both modalities of images, fast enhancing the brightness of low-light images by sharing parameters. The image enhancement process can be expressed as

$$I_{ir}^{en} = I_{ir} \odot L_{ir}, \quad (2)$$

$$I_{vi}^{en} = I_{vi} \odot L_{vi}, \quad (3)$$

where  $L_{ir}$  and  $L_{vi}$  denote the estimated illumination maps of infrared image  $I_{ir}$  and visible image  $I_{vi}$ , respectively.  $I_{ir}^{en}$  and  $I_{vi}^{en}$  denote the enhanced images. Besides, in this study, we estimate the illumination map in the RGB color space instead of the YCbCr space to effectively prevent color distortion during the inference process.

**Image Fusion Network.** In order to obtain a fusion image with more complementary features and better exposure status, we design an image fusion network with two novel modules, i.e., ADFM and STAM.

(a) ADFM. Inspired by [5] and [6], we first design a feature extraction block with skip connections to make use of the

features in multiple levels for comprehensive representation. In the feature fusion stage, we design the ADFM with the attention mechanism [7, 8] and the differential operation [2], in order to adjust brightness and reduce redundant information (please see Sec. 3 for detailed discussions). Specifically, to adaptively stress the importance of the features, the attention mechanism is introduced in ADFM and the attention map is constructed as

$$A_{tt} = \mathcal{S}(\text{Conv}_{3 \times 3}(\mathcal{F}_{ir}) \otimes \text{Conv}_{3 \times 3}(\mathcal{F}_{vi})). \quad (4)$$

where  $\mathcal{F}_{ir}$  and  $\mathcal{F}_{vi}$  represent the extracted multi-level feature maps of infrared and visible images, respectively. Further, we exploit  $A_{tt}$  and difference map of  $\mathcal{F}_{vi}$  and  $\mathcal{F}_{ir}$  to finely tune  $\mathcal{F}_{vi}$  and  $\mathcal{F}_{ir}$  as:

$$\tilde{\mathcal{F}}_{ir} = (\mathcal{S}(\mathcal{G}(\mathcal{F}_{vi} \ominus \mathcal{F}_{ir})) \odot (\mathcal{F}_{vi} \ominus \mathcal{F}_{ir}) \oplus \mathcal{F}_{ir}) \otimes A_{tt}, \quad (5)$$

$$\tilde{\mathcal{F}}_{vi} = (\mathcal{S}(\mathcal{G}(\mathcal{F}_{ir} \ominus \mathcal{F}_{vi})) \odot (\mathcal{F}_{ir} \ominus \mathcal{F}_{vi}) \oplus \mathcal{F}_{vi}) \otimes A_{tt}, \quad (6)$$

where  $\tilde{\mathcal{F}}_{ir}$  and  $\tilde{\mathcal{F}}_{vi}$  represent corrected feature.  $\mathcal{S}(\cdot)$ ,  $\mathcal{G}(\cdot)$  and  $\odot$  denote sigmoid function, average pooling and channel-wise multiplication, respectively. Then, the fused feature map  $\mathcal{F}_{fus}$  is obtained by

$$\mathcal{F}_{fus} = \text{Conv}_{3 \times 3}(\text{Cat}(\tilde{\mathcal{F}}_{ir}, \tilde{\mathcal{F}}_{vi})), \quad (7)$$

where  $\text{Cat}(\cdot)$  represents channel concatenation operation. Finally, the fusion image  $I_{fus}$  with different modalities of salient features is reconstructed from  $\mathcal{F}_{fus}$  by the decoder.

(b) STAM. Inspired by [9, 10, 11], in order to fully integrate the salient features of the infrared and visible images, we develop STAM to compute the saliency map of each image  $I$ , where the saliency value  $\mathcal{D}_I(x)$  at pixel  $x$  is computed as

$$\mathcal{D}_I(x) = \mathcal{H}_I(\mathcal{M}_p(x))^\top, \quad (8)$$

where  $\mathcal{M}_p(x) = [l_p^0, l_p^1, \dots, l_p^{255}] \in R^{1 \times 256}$  and  $l_p^i = (x - i)^p$ ,  $p$  is used to adjust the degree of objects' saliency.  $\mathcal{H}_I \in R^{1 \times 256}$  is the intensity histogram of image  $I$ .

**Loss Function.** The loss function for the illumination enhancement stage is identical to the one defined in work [4].

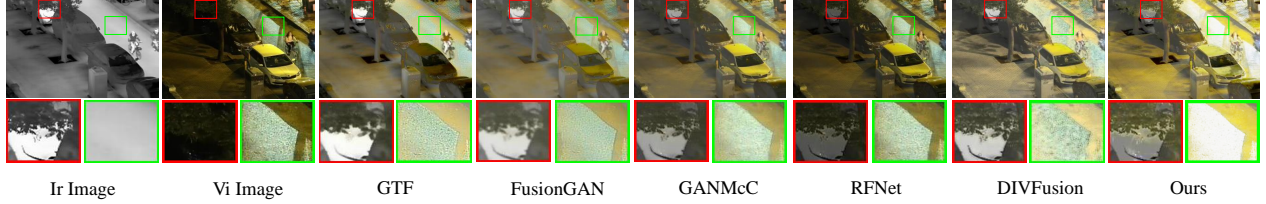


**Fig. 2.** Qualitative comparison of our IAIFNet and five state-of-the-art methods on fusing one pair of infrared and visible images (i.e., #190001). Under each image, two regions in the red and green boxes are zoomed in for clear comparison.

In the fusion stage, the loss function can be defined as

$$\mathcal{L}_{fus} = \alpha \mathcal{L}_{str} + \beta \mathcal{L}_{smooth}^{int} + \gamma \mathcal{L}_{grad}, \quad (9)$$

where  $\mathcal{L}_{str}$ ,  $\mathcal{L}_{smooth}^{int}$ , and  $\mathcal{L}_{grad}$  denote the structure loss, intensity consistent loss and gradient loss, respectively, and  $\alpha$ ,  $\beta$ , and  $\gamma$  are the corresponding hyperparameters to adjust their weights. Then,  $\mathcal{L}_{str}$  is formulated as

$$\mathcal{L}_{str} = 1 - SSIM(I_{fus}, \omega_{ir} \otimes I_{ir}^{en} + \omega_{vi} \otimes I_{vi}^{en}), \quad (10)$$

where  $\omega_{ir} = 0.5 + (\mathcal{D}_{I_{ir}^{en}} - \mathcal{D}_{I_{vi}^{en}}) / 2$ ,  $\omega_{vi} = 1 - \omega_{ir}$ ,  $\mathcal{D}_{I_{ir}^{en}}$  and  $\mathcal{D}_{I_{vi}^{en}}$  represent saliency maps of enhanced infrared and visible images, respectively.  $SSIM(A, B)$  calculates the structural similarity of images  $A$  and  $B$ . Thus,  $\mathcal{L}_{str}$  can supervise the network to transfer the diverse structural details from the infrared and visible images to the fusion image. Then,  $\mathcal{L}_{smo}^{int}$  is formulated as

$$\mathcal{L}_{smo}^{int} = \|I_{fus} - (\omega_{ir} \otimes I_{ir}^{en} + \omega_{vi} \otimes I_{vi}^{en})\|_1, \quad (11)$$

where  $\|\cdot\|_1$  denotes the  $l_1$ -norm. In this work for the fused images,  $\mathcal{L}_{smo}^{int}$  not only constrains the pixel-level intensity distribution but also assists our illumination enhancement network in suppressing the illumination information smoothly [12]. Finally,  $\mathcal{L}_{grad}$  is formulated as

$$\mathcal{L}_{grad} = \|\nabla I_{fus} - \max(\nabla I_{ir}^{en}, \nabla I_{vi}^{en})\|_1, \quad (12)$$

where  $\nabla$  and  $\max(\cdot)$  denote the Sobel gradient operator and elementwise-maximum selection operator, respectively. This gradient loss can supervise our model to preserve more salient edges and textures from the source images into the fusion image. In all experiments of this work,  $p$  is set to 2,  $\alpha$ ,  $\beta$ , and  $\gamma$  are set to 1, 15, and 3, respectively.

### 3. EXPERIMENTS

#### 3.1. Dataset and Implementation Details

In this study, 240 pairs of infrared and visible images from LLVIP [13] are used for training and 50 pairs for testing. The whole network is implemented based on PyTorch, trained on an NVIDIA RTX 3090 GPU, and the size of input image patches is set to  $600 \times 400$ . During the training of the illumination enhancement network, the batch size is set to 8, and the epoch number is set to 100. When training the image fusion network, the illumination-enhanced infrared and visible

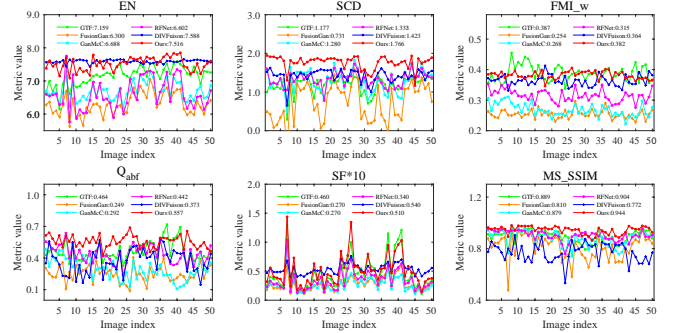


**Fig. 3.** Quantitative comparisons of different image fusion methods on 50 pairs of the image from the LLVIP dataset.

images are taken as its inputs, the batch size is set to 6, the epoch number is set to 150, and the initial learning rate is set to 0.001 and then decayed by 10 every 30 epochs. The Adam optimizer with momentum terms of  $\beta_1=0.9$  and  $\beta_2=0.999$  is exploited to optimize the parameters of our complete image fusion network.

#### 3.2. Performance Analysis

We conduct experiments against a series of state-of-the-art methods, including GTF [14], FusionGAN [15], GAN-McC [16], RFN-Nest [17], and DIVFusion [3], to verify the effectiveness of our IAIFNet.

**Qualitative Comparisons.** One comparison examples, performed on #190001 of LLVIP dataset, have been shown in Fig. 2. It can be seen that the fusion images of our IAIFNet are significantly better than those of other methods in terms of visual quality. Since GTF, FusionGAN, GANMcC and RFN-Nest do not consider the illumination condition of the source images, their results exhibit poor visual quality in terms of preserving contrast and details, as demonstrated by the red boxes in Fig. 2. In contrast, DIVFusion and our IAIFNet solve this issue well by exploiting the Retinex theory. However, the results of DIVFusion suffer from the over-exposure effect (further validated by the shadow of the tree in the green boxes) and contain lots of noise. As for our method, it can preserve more salient features while relieving artifacts owing to our intensity consistent loss, and thus outperforms other methods significantly in terms of qualitative evaluation.

**Quantitative Comparisons.** As shown in Fig. 3, we use six metrics to compare the quality of the fusion images produced

**Table 1.** The overall model size and inference time for processing 50 Pairs of images with Size  $256 \times 256$ .

Method	GTF	FusionGan	GANMcC	RFN-Nest	DIVFusion	Ours
Params(M) $\downarrow$	-	<b>1.982</b>	2.271	30.097	4.403	<b>0.635</b>
Time(s) $\downarrow$	-	0.677	1.295	0.246	<b>0.087</b>	<b>0.011</b>

**Table 2.** Multi-object detection results on the LLVIP dataset.

	Precision $\uparrow$	Recall $\uparrow$	mAP@.5 $\uparrow$		mAP@[.5:.95] $\uparrow$
			Person	Car	
Infrared	0.923	0.381	<b>0.769</b>	0.547	0.485
Visible	<b>0.924</b>	0.555	0.755	0.756	<b>0.589</b>
GTF	0.790	0.456	0.522	0.670	0.462
FusionGAN	0.782	0.426	0.490	0.657	0.439
GANMcC	0.791	<b>0.596</b>	0.531	0.799	0.526
RFN-Nest	0.802	<b>0.617</b>	0.535	<b>0.826</b>	0.544
DIVFusion	0.748	0.528	0.544	0.696	0.492
Ours	<b>0.986</b>	0.566	<b>0.770</b>	<b>0.787</b>	<b>0.612</b>

**Table 3.** Quantitative comparisons of different strategies.

E/Vis	E/Inf	ADFM	STAM	EN $\uparrow$	SCD $\uparrow$	FMI_w $\uparrow$	$Q_{abf}$ $\uparrow$	SF $\uparrow$	MS_SSIM $\uparrow$
$\times$	$\checkmark$	$\checkmark$	$\checkmark$	7.385	1.482	0.354	0.414	0.039	0.863
$\checkmark$	$\checkmark$	$\checkmark$	$\checkmark$	7.157	1.655	0.338	<b>0.578</b>	<b>0.059</b>	<b>0.943</b>
$\checkmark$	$\checkmark$	$\times$	$\checkmark$	<b>7.501</b>	<b>1.771</b>	0.369	0.547	<b>0.056</b>	<b>0.943</b>
$\checkmark$	$\checkmark$	$\checkmark$	$\times$	7.298	1.670	<b>0.401</b>	0.553	0.043	0.935
$\checkmark$	$\checkmark$	$\checkmark$	$\checkmark$	<b>7.516</b>	1.766	0.382	0.557	0.051	<b>0.944</b>

by different methods, including EN, SCD [18], FMI\_w [19],  $Q_{abf}$  [20], SF and MS\_SSIM [21]. The greatest values of SCD,  $Q_{abf}$ , and MS\_SSIM indicate that our fusion images preserve more structural information and higher contrast from the source images. Additionally, our method obtains the second-best results in terms of EN, SF, and FMI\_w.

**Computational Cost Comparison.** We evaluate the memory consumption and computation efficiency of the comparison methods. Specifically, the average inference time is computed for input images of size  $256 \times 256$ . As presented in Table 1, our model performs best in terms of both model size and inference speed.

### 3.3. Performance on Object Detection Task

To further explore the influence of our method on high-level vision tasks, we apply it to the multi-object detection task. We select YOLOv5 [22] as the baseline model to detect pedestrians and vehicles from the fusion images. As shown in Table 2, our method outperforms other methods on multi-object detection. Note that in terms of mAP@[.5:.95] on LLVIP, the detection results with our fusion images obtained 2.3% improvement compared to that only using visible images and performs better than those with fusion images of other methods. As shown in Fig. 4(a), the detection precision increases remarkably with our fusion images. Moreover, the detected results in Fig. 4(b) suggest that our fused images are more suitable for the detector to identify the objects.

### 3.4. Ablation Analysis

We design ablation experiments to test the effectiveness of the illumination enhancement network, ADFM and STAM,

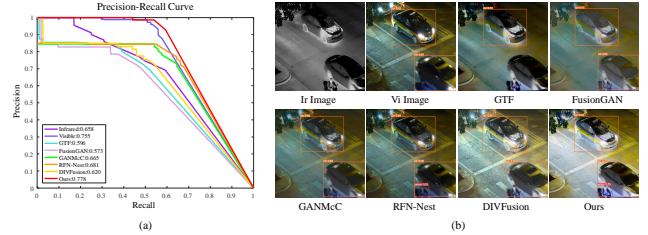


**Fig. 4.** Detection performance of our method in the dark environment. (a) The PR curves in mAP@.5. (b) Detection results on #220308.

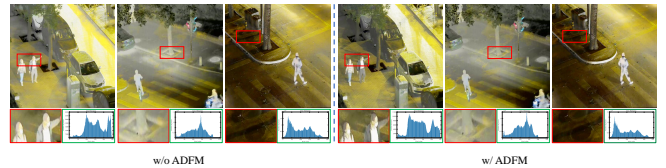


**Fig. 5.** Fusion images of our method with or without ADFM on #190271, #090161 and #210006, respectively.

as shown in Table 3, where “E/” indicates the illumination enhancement for corresponding image.

Visible image mainly describes the texture and contrast details of the image, which can be significantly amplified after illumination enhancement, resulting in an improvement in all 6 metrics. On the other hand, infrared images inherently possess the ability to express structural edge independent of illumination conditions, so that no changes result in relevant metrics  $Q_{abf}$  and SF. However, in order to achieve an optimal performance through all 6 metrics, which is the major focus in IVIF, illumination enhancement in both images is necessary. Fig. 5 demonstrates that the fusion image without using ADFM suffers the over-exposure defect, as indicated by the gray histograms in the green boxes. It can be seen from the zoomed-in areas (in red boxes) of the results that our fusion images demonstrate the best visual effect in terms of illumination distribution and detail visualization, indicating that the proposed ADFM can adaptively adjust the brightness of the fusion image and highlight its important details.

## 4. CONCLUSION

In this study, we propose a novel illumination-aware infrared and visible image fusion method, namely IAIFNet, which outperforms other SOTA methods, especially in low-light environments. Moreover, our method can not only improve the visual quality of the fusion image effectively through illumination estimation and enhancement, but also boost the performance of downstream multi-object detection tasks significantly.

## 5. REFERENCES

- [1] Yu Zhang, Lijia Zhang, Xiangzhi Bai, and Li Zhang, “Infrared and visible image fusion through infrared feature extraction and visual information preservation,” *Infrared Phys. Techn.*, vol. 83, pp. 227–237, 2017.
- [2] Linfeng Tang, Jiteng Yuan, Hao Zhang, Xingyu Jiang, and Jiayi Ma, “PIAFusion: A progressive infrared and visible image fusion network based on illumination aware,” *Inf. Fusion*, vol. 83–84, pp. 79–92, 2022.
- [3] Linfeng Tang, Xinyu Xiang, Hao Zhang, Meiqi Gong, and Jiayi Ma, “DIVFusion: Darkness-free infrared and visible image fusion,” *Inf. Fusion*, vol. 91, pp. 477–493, 2023.
- [4] Long Ma, Tengyu Ma, Risheng Liu, Xin Fan, and Zhongxuan Luo, “Toward fast, flexible, and robust low-light image enhancement,” in *CVPR*, 2022, pp. 5627–5636.
- [5] Hui Li and Xiao-Jun Wu, “Densefuse: A fusion approach to infrared and visible images,” *IEEE Trans. IP*, vol. 28, no. 5, pp. 2614–2623, 2019.
- [6] Han Xu, Jiayi Ma, Junjun Jiang, Xiaojie Guo, and Haibin Ling, “U2Fusion: A unified unsupervised image fusion network,” *IEEE Trans. PAMI*, vol. 44, no. 1, pp. 502–518, 2022.
- [7] Di Wang, Jinyuan Liu, Xin Fan, and Risheng Liu, “Unsupervised misaligned infrared and visible image fusion via cross-modality image generation and registration,” in *IJCAI*, 2022, pp. 3508–3515.
- [8] Zhishe Wang, Wenyu Shao, Yanlin Chen, Jiawei Xu, and Lei Zhang, “A cross-scale iterative attentional adversarial fusion network for infrared and visible images,” *IEEE Trans. CSVT*, vol. 33, no. 8, pp. 3677–3688, 2023.
- [9] Jinlei Ma, Zhiqiang Zhou, Bo Wang, and Hua Zong, “Infrared and visible image fusion based on visual saliency map and weighted least square optimization,” *Infrared Phys. Techn.*, vol. 82, pp. 8–17, 2017.
- [10] Jinyuan Liu, Yuhui Wu, Zhanbo Huang, Risheng Liu, and Xin Fan, “SMoA: Searching a modality-oriented architecture for infrared and visible image fusion,” *IEEE SPL*, vol. 28, pp. 1818–1822, 2021.
- [11] Jinyuan Liu, Xin Fan, Zhanbo Huang, Guanyao Wu, Risheng Liu, Wei Zhong, and Zhongxuan Luo, “Target-aware dual adversarial learning and a multi-scenario multi-modality benchmark to fuse infrared and visible for object detection,” in *CVPR*, 2022, pp. 5792–5801.
- [12] Chen Wei, Wenjing Wang, Wenhan Yang, and Jiaying Liu, “Deep retinex decomposition for low-light enhancement,” *arXiv:1808.04560*, 2018.
- [13] Xinyu Jia, Chuang Zhu, Minzhen Li, Wenqi Tang, and Wenli Zhou, “LLVIP: A visible-infrared paired dataset for low-light vision,” in *ICCV Workshop.*, 2021, pp. 3489–3497.
- [14] Jiayi Ma, Chen Chen, Chang Li, and Jun Huang, “Infrared and visible image fusion via gradient transfer and total variation minimization,” *Inf. Fusion*, vol. 31, pp. 100–109, 2016.
- [15] Jiayi Ma, Wei Yu, Pengwei Liang, Chang Li, and Junjun Jiang, “FusionGAN: A generative adversarial network for infrared and visible image fusion,” *Inf. Fusion*, vol. 48, pp. 11–26, 2019.
- [16] Jiayi Ma, Hao Zhang, Zhenfeng Shao, Pengwei Liang, and Han Xu, “GANMcC: A generative adversarial network with multiclassification constraints for infrared and visible image fusion,” *IEEE Trans. IM*, vol. 70, pp. 1–14, 2021.
- [17] Hui Li, Xiao-Jun Wu, and Josef Kittler, “RFN-Nest: An end-to-end residual fusion network for infrared and visible images,” *Inf. Fusion*, vol. 73, pp. 72–86, 2021.
- [18] V. Aslantas and E. Bendes, “A new image quality metric for image fusion: The sum of the correlations of differences,” *AEU Int. J. Electron. Commun.*, vol. 69, no. 12, pp. 1890 – 1896, 2015.
- [19] Mohammad Haghghat and Masoud Amirkabiri Razian, “Fast-FMI: Non-reference image fusion metric,” in *AICT*, 2014, pp. 1–3.
- [20] Costas S Xydeas, Vladimir Petrovic, et al., “Objective image fusion performance measure,” *Electron. Lett.*, vol. 36, no. 4, pp. 308–309, 2000.
- [21] Kede Ma, Kai Zeng, and Zhou Wang, “Perceptual quality assessment for multi-exposure image fusion,” *IEEE Trans. IP*, vol. 24, no. 11, pp. 3345–3356, 2015.
- [22] Joseph Redmon, Santosh Divvala, Ross Girshick, and Ali Farhadi, “You only look once: Unified, real-time object detection,” in *CVPR*, 2016, pp. 779–788.